Irregular Deep Ocean Wave Energy Conversion Using a Cycloidal Wave Energy Converter

Tiger Jeans
Mechanical Engineering, University of New Brunswick
15 Dineen Drive, Fredericton, New Brunswick, Canada
E-mail: tjeans@unb.ca

Casey Fagley
Atargis Energy Corporation, Pueblo, Colorado, United States
E-mail: casey.fagley@atargis.com

Stefan Siegel
Atargis Energy Corporation, Pueblo, Colorado, United States
E-mail: stefan.siegel@atargis.com

Jürgen Seidel
Atargis Energy Corporation, Pueblo, Colorado, United States
E-mail: jurgen.seidel@atargis.com

***Abstract*—The performance of a lift based wave energy converter in unidirectional irregular deep ocean waves is investigated. The energy converter consists of two hydrofoils attached parallel to a horizontal main shaft at a radius. The main shaft is aligned parallel to the wave crests and submerged at a fixed depth. The local flow field induced by the incident wave will cause the hydrofoils to rotate about the main shaft. The orientation of each hydrofoil is adjusted to produce the desired level of bound circulation. The energy converter and incident wave field are modeled using potential flow theory. The wave field is assumed to be long-crested and the hydrofoil span infinitely long, thereby the resulting flow field is two-dimensional. Each hydrofoil is modeled as a point vortex moving under a free surface. The irregular ocean wave is modeled by linear superposition of a finite number of regular wave components. The amplitude and frequency of each component is determined based on a Bretschneider spectrum. The hydrofoil position and bound circulation are controlled using a sensor located up-wave of the device and wave state estimator. The results demonstrate the converter's ability to effectively extract energy from multiple wave components simultaneously. Device efficiencies for incident wave fields consisting of 7 and 10 regular wave components were 85% and 77%, respectively.**

***Index Terms*—Ocean Wave Energy Conversion, Irregular Deep Ocean Wave, Cycloidal Wave Energy Converter, Feedback flow-control**

I. Introduction

The majority of existing ocean wave energy converters transform the wave energy into reciprocating mechanical motion, which then drives an intermediate power-take-off system that converters the energy to a useful form. However, it is possible to convert wave energy directly to rotational mechanical energy using a lift based energy converter consisting of one or more rotating hydrofoils aligned parallel with the incident wave crest [1]–[6]. The local flow field induced by the incident wave will cause the hydrofoils to rotate about the main shaft at the incident wave frequency [5]. The turbine efficiency is strongly dependent on the relative phase between the incident wave and hydrofoils and the bound circulation of each hydrofoil. Physically, circulation strength is related to the pitch angle of the hydrofoils and the local induced flow field.

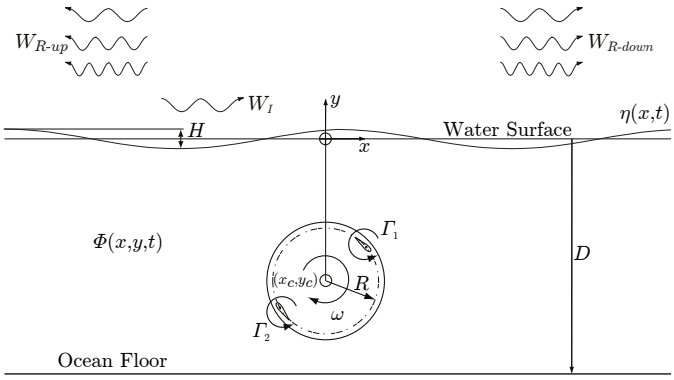

Fig. 1. Cycloidal wave energy converter geometry.

The geometry of this wave energy converter is similar to the well established Cycloidal or Voith-Schneider propeller, and is referred to as a Cycloidal Wave Energy Converter (CycWEC). A schematic of the CycWEC, as considered in this paper, is shown in Fig. 1. It features two hydrofoils with 180 degrees of phase attached parallel to a horizontally oriented main shaft at a radius R, rotating clockwise at angular speed ω, and submerged a depth y_c, which is measured relative to a Cartesian coordinate system with y = 0 being the undisturbed free surface. The hydrofoils are assumed to have infinite span in the third dimension, which is reasonable for hydrofoils having a large aspect ratio. They are also assumed to be aligned parallel with the incident wave crests. The orientation (pitch) of each hydrofoil may be adjusted to produce the desired level of circulation Γ. At any point on the free surface the vertical elevation is η and peak-to-peak amplitude of the resulting wave field is H. The incoming ocean wave W_I is assumed to travel left to right, and waves generated by the CycWEC traveling in the direction of the incoming wave are considered traveling in the down-wave direction and are identified as W_{R-down}; while waves traveling in the opposite direction are considered traveling up-wave and are identified as W_{R-up}.

The CycWEC concept was first investigated in the late

1980s by researchers at TU Delft University [4]–[6]. Experiments conducted at MARIN using a single hydrofoil attached to a submerged horizontal shaft verified that the device could operate as a winch in regular long crested waves. The concept was further investigated both experimentally in [4] and numerically in [6]. This initial work demonstrated the feasibility of the approach, as well as the ability of the CycWEC to self-synchronize with the incoming wave frequency and rotational phase. However, the conversion efficiencies found both in the theoretical work and the wave tunnel experiments were very small, on the order of few percent in experiments, with a theoretical maximum of 15%.

Recent research at the United States Air Force Academy (USAFA) has focused on extending the original work conducted at TU Delft [1]. The primary objective is to increase the device efficiency by operating at significantly higher blade speeds than the wave-induced velocity and by using feedback flow-control to intelligently control the turbine blade orientation and position based on the incident wave field. Initially, computational simulations were performed in [1] and [2] with the device operating as a wave generator with a constant rotational rate and bound circulation. This verified that the CycWEC primarily produces a single-sided wave field and thus is well suited for operation as a wave termination device. The resulting wave field was composed of three components, the fundamental wave and its first two harmonics. The frequency of the fundamental wave matched the rotational frequency of the CycWEC and the amplitude was proportional to the hydrofoil bound circulation. For a given bound circulation, the wave amplitude decreased nonlinearly as the device submergence depth increased.

The study also showed that resulting wave amplitudes are strongly dependent on the device radius, which, for a given rotational frequency, is proportional to blade speed. The fundamental wave amplitude was maximized when $2R/\lambda = 1/\pi$, where λ is the fundamental wave length. It was also determined that by using a configuration with two hydrofoils of opposite circulation and 180 degrees of phase the first harmonic from each wave canceled. This was a significant finding because, as noted in [5], the potential of the device was limited by the fact that the amplitude of the generated harmonic waves became increasingly significant as the device was situated closer to the free surface, which is the same region where the device becomes an efficient wave generator.

Wave cancellation of both deep and intermediate long crested regular ocean waves was successfully demonstrated in [1] and [2]. To operate as an effective wave termination device the motion of the CycWEC was synchronized in frequency and phase locked to the incoming wave. The circulation of the hydrofoils was adjusted to produce the same wave amplitude as the incoming wave. Inviscid simulations resulted in device efficiencies in excess of 99%.

Preliminary wave generation and cancellation experiments at a 1/300 scale have been conducted at USAFA and the results can be found in [7]. For the wave cancellation experiments the regular incident wave field is known and the CycWEC was synchronized according. In general, the results from the experiments agree well with the computational results in [1] and [2]. More recently, small scale experiments with regular wave cancellation employing both state estimation and feedback control have been completed.

Real ocean waves are random in nature with wave patterns that are ever changing in both time and space. This will require significantly more complex feedback flow-control algorithms for the CycWEC to operate efficiently as an ocean wave energy converter. The hydrofoil bound circulation, device phase and rotational frequency must continuously vary. As such, the objective of this paper is to numerically investigate the performance of a CycWEC in unidirectional long crested irregular ocean waves.

II. Computational Model

The CycWEC and wave-induced flow field are modeled using potential flow theory. For an inviscid, incompressible, and irrotational flow, the governing continuity equation simplifies to the Laplace equation,

$$\nabla^2 \Phi = 0 \tag{1}$$

where Φ is the velocity potential. Unique solutions to Equation 1 are determined by satisfying the appropriate boundary conditions based on physical considerations. In seeking two-dimensional solutions it is often convenient to define the complex stream function in terms of the complex coordinate $z = x + iy$,

$$F(z,t) = \Phi + i\Psi \tag{2}$$

where Ψ is the stream function and the complex velocity is defined by $dF/dz = u - iv$.

A. Cycloidal Wave Energy Converter Model

The simplest representation of a two-dimensional hydrofoil that correctly represents the flow induced in the far field is a point vortex of strength Γ equal to the hydrofoil bound circulation. When the hydrofoil is in the presence of a free surface it is imperative that the appropriate kinematic and dynamic boundary conditions be satisfied on that surface. Derivations of the linearized free surface boundary condition can be found in [8]. Neglecting higher order terms, the kinematic boundary condition ensuring the vertical velocity of the free surface and the fluid are equal is,

$$\frac{\partial \eta}{\partial t} = \frac{\partial \Phi}{\partial y}. \tag{3}$$

The dynamic boundary condition ensuring the pressure on the free surface is atmospheric is determined from Bernoulli's equation. Substituting the free surface elevation for y, and again neglecting higher order terms results in,

$$\eta = -1/g \frac{\partial \Phi}{\partial t}, \tag{4}$$

where $g = 9.81$ m/s is the gravity constant. Due to the linearization, Equation 4 can be imposed at $y = 0$. A non-reflective boundary condition is applied at the domain boundaries to avoid wave reflections.

Subject to the above boundary conditions, the complex potential for a vortex moving under a free surface with position $c(t) = x(t) + iy(t)$ in the complex plane is developed in [9] to be,

$$\begin{aligned} F(z,t) &= \frac{\Gamma(t)}{2\pi i} ln\left(\frac{z-c(t)}{z-\bar{c}(t)}\right) \\ &+ \frac{g}{\pi i}\int_0^t \int_0^\infty \frac{\Gamma(\tau)}{\sqrt{gk}} e^{-ik(z-\bar{c}(\tau))} \\ &\times sin\left[\sqrt{gk}(t-\tau)\right] dkd\tau \end{aligned} \quad (5)$$

where $\Gamma(t)$ is the circulation of the vortex, and k the wave number. The first term is the complex potential due to the vortex and its mirror image above the surface, which is necessary to satisfy the kinematic free surface condition. The second term describes the radiated waves related to the dynamic free surface condition. It is also important to note that in Equation 5 the fluid is assumed to be infinitely deep.

Each CycWEC hydrofoil is modeled by numerically integrating Equation 5 using a second order time and wave number marching technique. To ensure that the numerical solution sufficiently converges, numerical integration settings for Δt, Δk, and k_{max} were chosen based on the results of the convergence study presented in [1]. Equation 4 is then used to determine the resulting surface elevation and wave pattern. The theory of superposition is used to extend this approach to a CycWEC with two hydrofoils, where the total potential is determined from $\Phi_{total} = \sum_{i=1}^{2} \Phi_i$ and Φ_i is the potential of each hydrofoil.

The position of each hydrofoil is a function of the instantaneous incident wave field and is determined from the implemented feedback flow-control scheme. The coordinates for the first hydrofoil moving about the center of rotation $(0, y_c)$ with radius R is,

$$\begin{aligned} x_1(t) &= R\cos[\phi(t)] \\ y_1(t) &= y_c - R\sin[\phi(t)], \end{aligned} \quad (6)$$

and for the second hydrofoil is,

$$\begin{aligned} x_2(t) &= R\cos[\phi(t)+\pi] \\ y_2(t) &= y_c - R\sin[\phi(t)+\pi], \end{aligned} \quad (7)$$

where ϕ is the angular position of the first hydrofoil measured clockwise from the y-axis.

The hydrofoil bound circulation $\Gamma(t)$ is a function of the instantaneous wave height and is also determined from the implemented feedback flow-control scheme. It should be noted that no wake model is implemented to ensure that Kelvin's conditions is satisfied at each time step. In actuality each hydrofoil would shed vorticity into its wake of an amount equal to the change in bound circulation. Thin hydrofoil simulations presented in [1] showed that this effect is negligible for far field estimates of surface elevation when the hydrofoil chord is small relative to the wave length (i.e., $c/\lambda << 1$).

B. Irregular Wave Model

The irregular incident wave field is modeled using a linear superposition of a finite number of linear Airy wave components. The velocity potential for a unidirectional deep ocean wave propagating in the x-direction and satisfying the linearized free surface boundary conditions is given in [8] to be,

$$\Phi_{Airy}(x,y,t) = \frac{Hg}{2\omega} e^{ky} sin\left(kx - \omega t + \theta\right) \quad (8)$$

where H is the peak-to-peak wave amplitude, ω is the wave frequency, k is the wave number and θ is a random phase angle. Thus, the velocity potential for the unidirectional irregular incident wave field is given by,

$$\Phi_I(x,y,t) = \sum_{i=1}^{N_I} \frac{H_i g}{2\omega_i} e^{k_i y} sin\left(k_i x - \omega_i t + \theta_i\right) \quad (9)$$

and the resulting surface elevation is,

$$\eta_I(x,t) = \sum_{i=1}^{N_I} \frac{H_i}{2} cos\left(k_i x - \omega_i t + \theta_i\right), \quad (10)$$

where N_I is the number of regular wave components used to represent the irregular wave field, and H_i, k_i, ω_i and θ_i are the wave height, number, frequency and phase for component i, respectively. The wave phase components θ_i are obtained using a random number generator based on a uniform distribution between 0 and 2π. The fidelity of the irregular wave field will increase as the number of wave components is increased. According to [10], a minimum of 20 wave components are required for modeling a unidirectional irregular seaway.

The amplitude for component i is based on a specified wave spectrum according to,

$$a_i = \frac{H_i}{2} = \sqrt{2 S_I(\omega_i)\Delta\omega_i}, \quad (11)$$

where S_I is the spectral density and $\Delta\omega_i$ is the wave frequency interval for component i.

For the current study the the incident wave field is modeled using the Bretschneider wave spectrum, which is a commonly used two parameter model for wave spectra in the open ocean. The 15th International Towing Tank Conference [11] defines the Bretschneider spectrum as,

$$S_I(\omega) = \frac{486.0 H_s^2}{T_p^4 \omega^5} \exp\frac{-1948.2}{T_p^4 \omega^4}, \quad (12)$$

where H_s is the significant wave height and T_p is the wave period associated with the peak energy. The Bretschneider wave spectrum for $H_s = 3.25$ m and $T_p = 9.7$ s (i.e. sea-state 5) is shown in Fig. 2(a). Also shown are the resulting wave components when the spectrum is divided into 21 wave components with $\omega_{min} = 0.4$ rad/s, $\omega_{max} = 2.0$ rad/s,

and $\Delta\omega_i = 0.08$ rad/s. Each wave component is identified numerically in Fig. 2(a) and are identified as $W_{I1} - W_{I21}$ throughout the remainder of the paper. The amplitude of each wave is determined from Equation 11.

With the period and amplitude of each component wave defined, the associated wave length and power can be determined from Airy wave theory. The wave length is determined from the dispersion relationship as follows,

$$\lambda_i = \frac{T_i^2 g}{2\pi}, \tag{13}$$

where λ_i and T_i are the wavelength and period of component i. The wave power per unit length, P_i, associated with each component is related to the wave height and period by,

$$P_i = \frac{1}{32\pi}\rho g^2 H_i^2 T_i, \tag{14}$$

where ρ is the density of water (assumed to be $\rho = 1000$ kg/m^3 for this study). Since the wave power scales linearly with the wave period, higher harmonic waves of the same wave height will contain less energy in proportion to their period. Also note the quadratic relationship between wave energy and wave height. The power associated with each component wave in Fig. 2(a) is shown in Fig. 2(b). The total power of all 21 components is 41.79 kW/m and W_{I4} has the peak power of all individual components with 8.75 kW/m.

C. Feedback Flow Control Model

For the successful cancellation of an unknown, incoming airy wave, feedback control and wave state estimation are necessary. Algorithms to interpret and estimate the wave state in real time fashion are needed to adequately control and efficiently extract energy. The wave state for a single Airy wave is defined as phase ϕ, frequency ω, and wave height H. A sensor which measures the wave height over time is placed upstream of the CycWEC. This measurement is defined as $\eta(t)$ and displays purely a periodic signal with unknown frequency and amplitude and is also corrupted by a small amount of high frequency noise. The implemented feedback control scheme is shown in Figure 3. The sensor relays a signal to the estimator which estimates the wave height, phase and period. The controller then computes the rotational position and blade angle to generate an opposing wave that effectively cancel the incident wave field.

Given a time history of the upstream measurement a relation is sought such that $[\hat{\omega}(t)\hat{\phi}(t)\hat{H}(t)]^T = fcn\left([\eta(t), \eta(t-1), \ldots, \eta(t-n)]\right) + e(t)$ with minimal estimation error, $e(t)$. A typical Fourier analysis falls short because instantaneous phase information is lost in the decomposition. Therefore, other digital signal processing methods need to be implemented. Because the up-wave wave height measurement contains no negative frequency components, the signal can be expressed as an analytic signal such that,

$$\eta(t) = \frac{1}{2\pi}\int_0^\infty \eta(\omega) e^{j\omega t} d\omega. \tag{15}$$

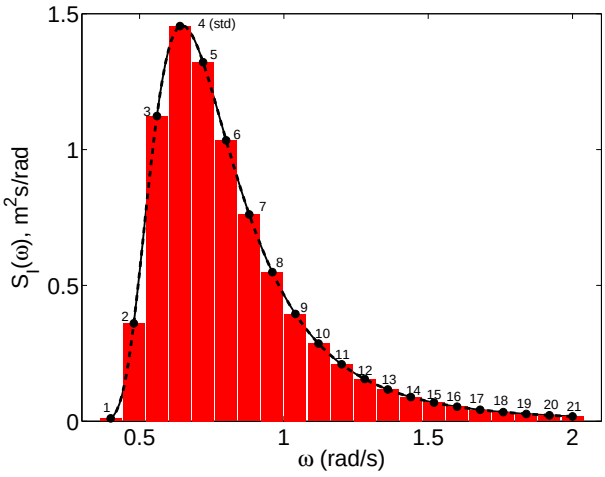

(a) Bretschneider energy spectrum for $H_s = 3.25$ m and $T_p = 9.7$ s (i.e. sea-state 5).

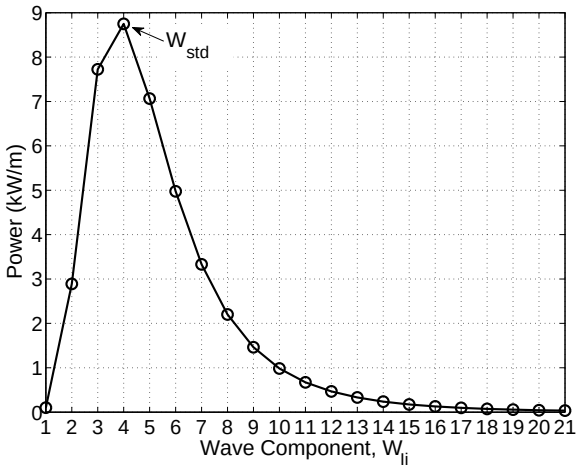

(b) Associated power of each of the 21 discrete wave components.

Fig. 2. Incident wave field modeled using the Bretschneider wave spectrum and 21 discrete wave components based on Airy wave theory.

A complex representation of a periodic signal is $e^{j\omega t} = \eta(t) + i\hat{\eta}(t)$. The complex component of the analytic signal, which is unknown at this point, is analogous to the Hilbert transformation,$\mathcal{H}[\bullet]$, of the real component; that is $\hat{\eta}(t) = \mathcal{H}[\eta(t)]$. The Hilbert transformation is a linear filter which produces a phase shift of $\pm\frac{\pi}{2}$ over all frequencies present in the signal, $\eta(t)$. In the time domain the transformation for this linear filter is identically the convolution with $\frac{1}{\pi t}$ which is shown as,

$$\mathcal{H}[\eta(t)] = \frac{1}{\pi t} * \eta(t) = \frac{1}{\pi}\int_{-\infty}^{\infty} \frac{\eta(t-\tau)}{\tau} d\tau. \tag{16}$$

In the frequency domain the transform of the signal $f = \frac{1}{\pi t}$ is

$$-jsgn(f) = \begin{cases} -jf > 0 \\ 0f = 0 \\ jf < 0 \end{cases} \tag{17}$$

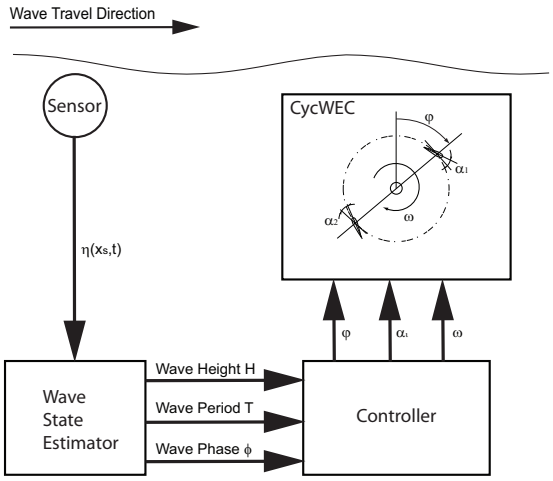

Fig. 3. Block diagram of the implemented feedback flow control scheme for the cycloidal wave energy converter.

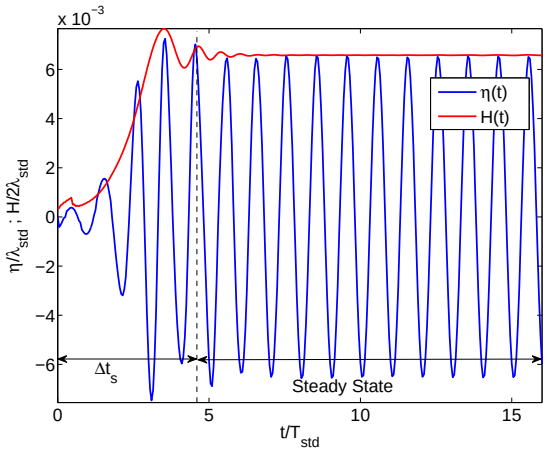

Fig. 4. Surface Elevation at $x = \lambda_{std}$ for a wave generation simulation with $T/T_{std} = 1.0$ and $\Gamma T_{std}/\lambda_{std} = 0.0043$.

The transfer function of this ideal filter will have a magnitude of one and phase of $\pm\frac{\pi}{2}$ for $\pm\omega$, respectively. Because the Fourier transform is a non-causal transformation (dependent on previous, current and future measurements), an approximation to this transformation is necessary. Typical filters such as finite impulse response (FIR) and infinite impulse response (IIR) filters can be designed to simulate the response of $\frac{1}{\pi t}$. As for the purposes of this paper a 3 stage cascading IIR filter is used to estimate the complex component of the Hilbert transformation with minimal phase (although non-linear) delays at the designed frequency.

Now that the real and complex components of the analytic signal are known to some degree of error, the instantaneous amplitude is estimated from the L_2 norm of the signals, (i.e., $\hat{H}(t) = \|\eta(t) + \hat{\eta(t)}\|_2$). The instantaneous phase is then computed as the angle between the real and complex estimate as, $\hat{\phi}(t) = \arctan(\frac{\hat{\eta}(t)}{\eta(t)})$. The instantaneous frequency is the time derivative of the phase estimate.

As seen in Fig. 3, the wave state is now fully estimated. The control scheme is very basic for the purposes of this paper. Proportional control is used for the blade pitch (i.e., bound circulation), such that $\alpha_i(t) = P_{gain}\hat{H(t)}$. This is a reasonable assumption as open loop wave generation results shown in [1] display a very linear relationship between the bound circulation and resulting wave height. As for rotary control of the propeller the group velocity is estimated and compensated for as a phase delay. The time delays are then superimposed to control the rotational velocity of the main shaft in a stepwise fashion, such that $\theta(t) = \phi(t) + \frac{\eta_\lambda}{C_g} + \theta_f$, where C_g is the group velocity of the wave, and θ_f is the phase compensation of the Hilbert transformation filter.

III. Results and Discussion

The majority of the energy in the Bretschneider spectrum (and other theoretical and measured ocean wave energy spectra) is contained in the low frequency, large wave length components; therefore, it is imperative that the CycWEC perform well in this region. As such, wave components $W_{I1} - W_{I10}$ in Fig. 2, which contain 95% of the total energy in all 21 wave components, are considered in the current study. If deemed necessary, future investigations may consider the effects of all 21 wave components. Since W_{I4} contains the peak power of all discrete waves considered, it is refered to as the standard wave and identified as W_{std}. The standard period, wave length and amplitude are defined as $T_{std} = 9.817$ s, $\lambda_{std} = 150.48$ m, and $a_{std} = 0.48$ m . The CycWEC design parameters are optimized for extracing energy from the standard wave based on the result presented in [1]. In particular, the device radius was chosen such that $R/\lambda_{std} = 1/2\pi$ and the device submergence depth is fixed at $y_c/\lambda_{std} = -0.1632$.

A. Wave Generation

To achieve wave cancellation, the wave generated by the CycWEC in the down-wave direction must match the incident wave amplitude and period, while being exactly out of phase. To ensure that a CycWEC optimized for W_{std} can extract energy from wave components $W_{I1} - W_{I10}$, an initial investigation of the wave generation properties as a function of the device rotational period was conducted. The hydrofoil bound circulation was held constant for all simulations at $\Gamma T_{std}/\lambda_{std}^2 = 0.0043$ and the CycWEC period was varied to match each of the 10 wave components in the Bretschneider spectrum considered, (i.e., $T = T_i$ for $i = 1 - 10$). The resulting transient and steady state surface elevations at $x = \pm\lambda_{std}$ were determined for each case.

The generated wave pattern as a function of time at $x = \lambda_{std}$ is shown in Fig. 4 for the design case of $T/T_{std} = 1.0$. Also shown is the resulting fundamental wave height of the generated wave as a function of time, $H(t)$. After several rotations of the CycWEC the free surface becomes periodic in time, and is referred to as a steady state wave pattern. As indicated in the figure, $H(t)$ was used to determine the time necessary to achieve a steady state wave pattern, Δt_s. Both Δt_s and $H(t)$ varied with the CycWEC period.

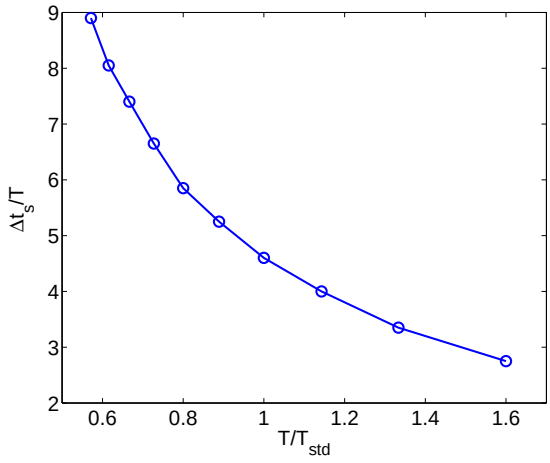

Fig. 5. Time required to achieve a steady state wave field $x = \lambda_{std}$ as a function of CycWEC period. Results shown for all wave generation simulations with $y_c/\lambda_{std} = -0.1632$, $R/\lambda_{std} = 1/2\pi$ and $\Gamma T_{std}/\lambda_{std}^2 = 0.0043$.

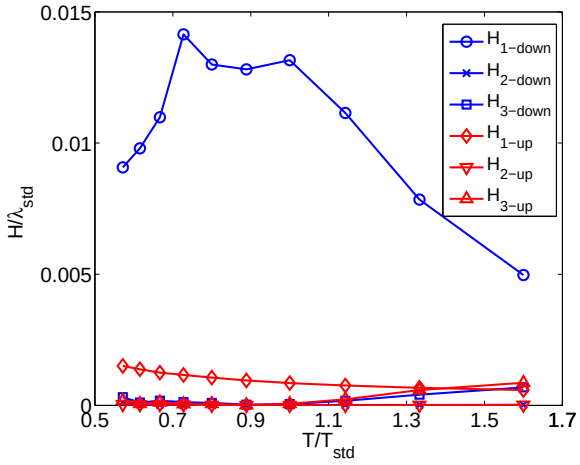

Fig. 6. Wave height of the fundamental, 1^{st}, and 2^{nd} harmonic waves based on an FFT analysis of the resulting wave field at $x = \pm\lambda_{std}$ for all wave generation simulations.

The time to achieve a steady state wave pattern at $x = \lambda_{std}$ was determined for each simulation and is plotted in Fig. 5. As the device period is decreased the total number of revolutions necessary to reach steady state increases nonlinearly. When $T/T_{std} = 0.57$ (i.e., W_{I10}) 9 complete revolutions are necessary to reach steady state. This result will introduce additional complexity in the feedback control scheme when canceling a dynamic irregular wave field.

A Fast Fourier Transform (FFT) analysis was performed on the generated steady state wave fields at $x = \pm\lambda_{std}$ to decompose the resulting wave field into its components. For all simulations the FFT analysis showed that the CycWEC generates a fundamental wave having a period equal to the CycWEC and the 2^{nd} harmonic having a period of $T/3$. This is in agreement with the results of [1], which showed that for the current configuration the 1^{st} harmonic wave from each hydrofoil cancels in both the up- and down-wave directions and no higher harmonic waves are generated. The relative amplitudes of the fundamental and harmonic waves at $x = \pm\lambda_{std}$ is shown in Fig. 6, where the fundamental and first two harmonic waves are identified as H_1, H_2, and H_3, respectively. Note that for all cases the dominant wave amplitude is H_{1-down}, indicating that a single CycWEC can potentially efficiently extract energy from incident waves ranging in frequency from $\omega = 0.4 - 1.2$ rad/s.

B. Wave Cancellation

The interaction between the CycWEC and the incident wave field is modeled by linearly combining the velocity potentials given in Equations 5 and 9. The surface elevation is subsequently determined using Equation 4. To achieve effective energy extraction the position of the CycWEC hydrofoils and bound circulation are controlled using the feedback control scheme described in Section II.C. The sensor for the wave state estimator is located up-wave at $x = -\lambda_{std}$. The objective is to optimally control the hydrofoil circulation and angular position such that the CycWEC extracts energy from the various wave components simultaneously.

The primary variable of merit for the CycWEC design is the percentage of the wave energy extracted from the incident wave field, defined as the device hydrodynamic efficiency, ϵ. The efficiency is determined from a control volume analysis based on energy conservation which is implicit in the unsteady Bernoulli equation. The analysis assumes that all energy leaving or entering at the up–wave and down–wave boundaries is contained in traveling Airy type waves. Thus, the power difference at both boundaries is to be provided or absorbed by the CycWEC hydrofoils. The domain boundaries are located at $\pm\lambda_{std}$. The hydrodynamic efficiency is defined as,

$$\varepsilon = 1 - \frac{|P_I - P_{R-up}| + P_{R-down}}{P_I}, \qquad (18)$$

where P_I is the power contained in the incident wave field at the up-wave boundary without the turbine, P_{R-up} and P_{R-down} are the power contained in the resulting wave fields at the up-wave and down-wave boundaries, respectively, with the CycWEC operating. The hydrodynamic efficiency will reach a value of one when the incident wave field at the up-wave boundary is undisturbed by the CycWEC and the wave field at the down-wave boundary approaches zero.

The resulting wave fields at the up- and down-wave boundaries (i.e., $x = \pm\lambda_{std}$) are reconstructed using a FFT. To ensure that initial transients did not affect the analysis, data prior to $t/T_{std} = 10$ was discarded. To determine the total power in the wave fields P_{R-up} and P_{R-down}, each wave component identified in the FFT was assumed to be an Airy type and its associated power was determined from Equation 14. The resulting hydrodynamic efficiency was then determined using Equation 18.

1) Two-Component Incident Wave: An initial assessment of the CycWEC controller was performed by investigating the performance with an incident wave field consisting of two

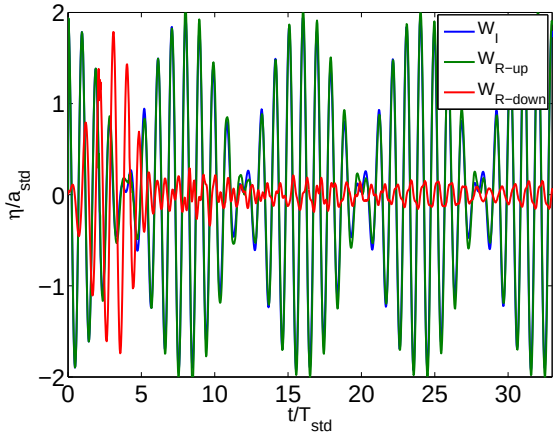

Fig. 7. Resulting surface elevation for a two-component incident wave with $W_I = W_{I5} + W_{std}$ and $\theta_5 = 90$ degrees. Resulting wave patterns are shown at the up- and down-wave domain boundaries where $x = \pm\lambda_{std}$.

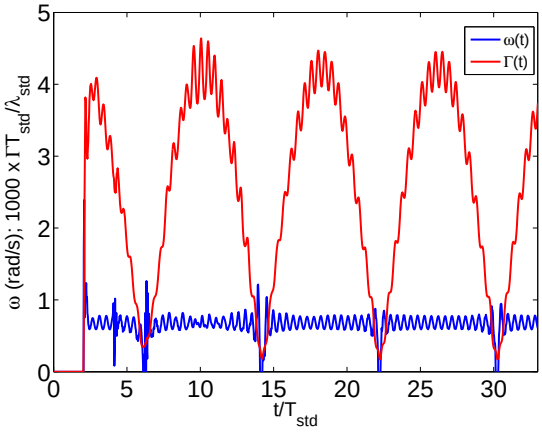

Fig. 8. Circulation and angular rotation rate of the hydrofoils for a two-component incident wave with $W_I = W_{I5} + W_{std}$ and $\theta_5 = 90$ degrees.

regular wave components where $W_I = W_{Ii} + W_{std}$ with $i = 1-3$ and $5-10$. For each incident wave field combination the phase between the component waves was varied as follows, $\theta_{std} = 0$ degrees and $\theta_i = 0, 45, 90,$ and 13 degrees.

Typical resulting wave patterns as a function of time at $x = \pm\lambda_{std}$ are shown in Fig. 7. The case shown is for the incident wave field $W_I = W_{I5} + W_{std}$ and $\theta_5 = 90$ degrees. Note that the resulting and incident wave fields at the up-wave boundary are nearly identical and the resulting wave field at the down-wave boundary has been significantly reduced, indicating that a significant portion of the energy in the incident wave field has been absorbed by the blades of the CycWEC. For this particular case the hydrodynamic efficiency was determined using Equation 18 to be $\epsilon = 0.92$.

It was shown in [1] that for effective energy extraction from a given regular deep ocean wave both the CycWEC hydrofoil bound circulation and angular speed are constant. However, as previously outlined, for an irregular incident wave field the hydrofoil bound circulation must be directly controlled and the blade angular speed must be indirectly controlled (through angular position ϕ) in real time using up-wave measurements of the surface elevation. The resulting bound circulation and blade angular speed as functions of time for the case presented in Fig. 7 are shown in Fig. 8. This highlights the additional complexity of effective energy extraction from an incident wave field consisting of just two Airy waves with similar frequency and random phase.

To determine the wave components in the resulting wave field at the up- and down- wave boundary an FFT analysis was performed on each two-component incident wave simulation. The results for each simulation with $\theta_i = 90$ degrees are shown in Fig.9. Figures 9(a) and 9(b) highlight that when the incident wave field consists of the standard wave and a low frequency, low energy, wave component the controller generates a resulting wave field that primarily cancels the standard wave and the low frequency wave passes relatively undisturbed. Figure 9(c) - 9(f) highlight that when the incident wave field consists of two wave components with similar frequency, both carrying a significant portion of the total energy, the controller generates a wave field that effectively cancels both components in the incident wave field simultaneously. Figures 9(g)-9(i) highlight that when the incident wave field consists of the standard wave and a high frequency, low energy, wave component the controller generates a resulting wave field that primarily cancels the standard wave and the high frequency wave passes relatively undisturbed. This behavior is expected because the controller is optimized for extracting energy from the high energy waves near the peak of the Bretschneider spectrum. Importantly, the low and high frequency waves that carry less energy do not "confuse" the controller, and the CycWEC is still able to effectively cancel the high energy carrying wave.

The hydrodynamic efficiency for each of the two-component wave simulations was determined using Equation 18 and the results are shown in Fig. 10. The results have been plotted separately for each of the relative phase angles, θ_i, investigated. With the exception of the results for $W_I = W_{I6} + W_{std}$ and $\theta_6 = 0$ and 45 degrees, for all simulations with $T_i/T_{std} > 0.72$ the hydrodynamic efficiencies are in excess of $\epsilon = 0.8$ and the maximum efficiency achieved was $\epsilon = 0.97$. For simulations with $T_i/T_{std} < 0.72$ the hydrodynamic efficiency is reduced because, as previously noted, the CycWEC does not cancel the high frequency wave. The hydrodynamic efficiency was dependent on the relative phase between the two component waves and the cause of this result is still unknown and requires further investigation. Overall, these results demonstrate the CycWEC's ability to effectively extract energy from multiple wave components simultaneously through intelligent control of the hydrofoil pitch and position. Thus the CycWEC has the potential to operate effectively in irregular deep ocean waves.

2) Multi-Component Incident Wave: To determine if the CycWEC is effective as extracting wave energy from a more realistic irregular unidirectional deep ocean wave field, sim-

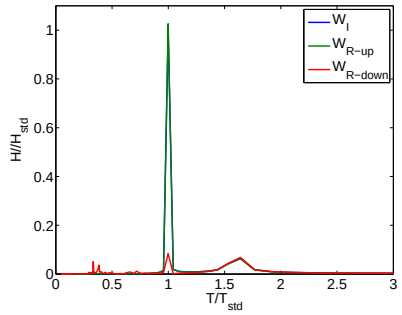

(a) FFT analysis of incident and resulting wave fields for $W_I = W_{I1} + W_{std}$ and $\theta_1 = 90$ degrees.

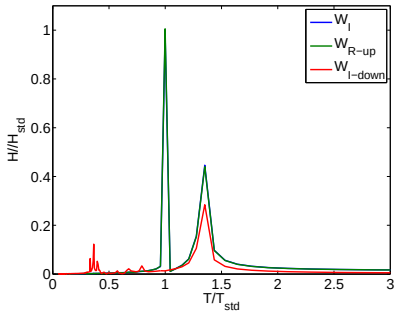

(b) FFT analysis of incident and resulting wave fields for $W_I = W_{I2} + W_{std}$ and $\theta_2 = 90$ degrees.

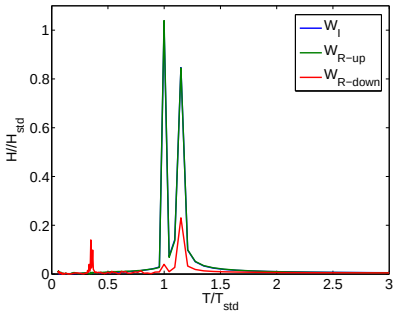

(c) FFT analysis of incident and resulting wave fields for $W_I = W_{I3} + W_{std}$ and $\theta_3 = 90$ degrees.

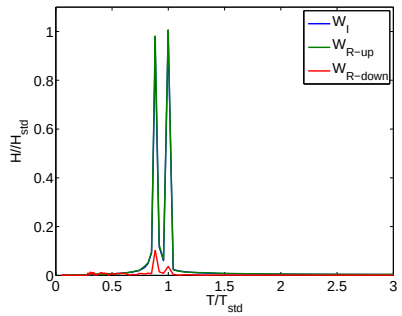

(d) FFT analysis of incident and resulting wave fields for $W_I = W_{I5} + W_{std}$ and $\theta_5 = 90$ degrees.

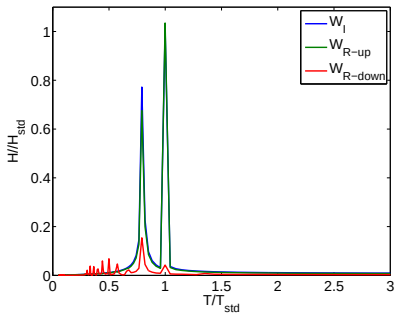

(e) FFT analysis of incident and resulting wave fields for $W_I = W_{I6} + W_{std}$ and $\theta_6 = 90$ degrees.

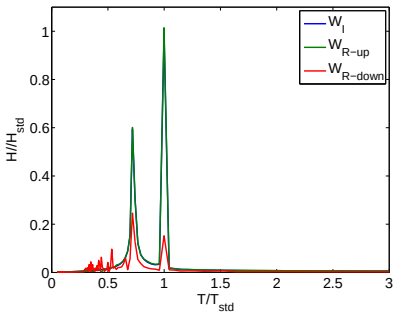

(f) FFT analysis of incident and resulting wave fields for $W_I = W_{I7} + W_{std}$ and $\theta_7 = 90$ degrees.

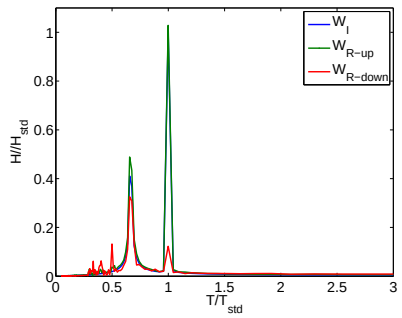

(g) FFT analysis of incident and resulting wave fields for $W_I = W_{I8} + W_{std}$ and $\theta_8 = 90$ degrees.

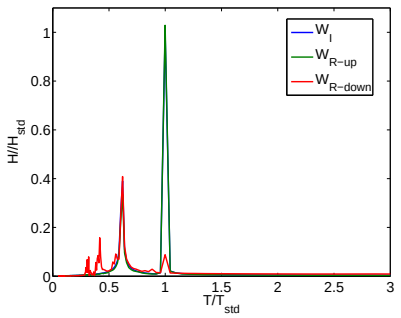

(h) FFT analysis of incident and resulting wave fields for $W_I = W_{I9} + W_{std}$ and $\theta_9 = 90$ degrees.

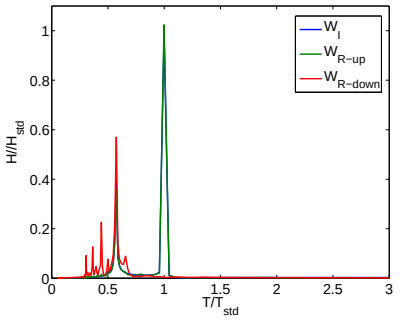

(i) FFT analysis of incident and resulting wave fields for $W_I = W_{I10} + W_{std}$ and $\theta_{10} = 90$ degrees.

Fig. 9. FFT analysis of incident and resulting wave fields for two-component simulations with $\theta_i = 90$ degrees and $\theta_{std} = 0$ degrees.

ulations were completed with incident wave fields consisting of 7- and 10-components waves. The 7-component incident wave was defined as $W_I = \sum_{i=1}^{7} W_i$ and the 10-component incident wave was defined as $W_I = \sum_{i=1}^{10} W_i$, where each component W_i was defined in Fig. 2. The phase, θ_i, for each component was determined using a random number generator based on a uniform distribution between 0 and 2π. Results for the 7-component incident wave simulation are shown in Fig. 11 and for the 10-component incident wave simulation are shown in Fig. 12.

Plotted in Fig. 11(a) and 12(a) are the incident and resulting wave patterns at $x = \pm\lambda_{std}$. Note that for both simulations the resulting and incident wave fields at the up-wave boundary are very similar and the resulting wave field at the down-wave boundary has been reduced, indicating that a significant portion of the energy in the incident wave field has been extracted by the CycWEC.

Time histories of bound circulation and blade angular speed are plotted in Fig. 11(b) and 12(b) for each respective simulation. For both simulations the bound circulation and angular speed are significantly more complex and random than the distributions shown previously in Fig. 8 for the 2-component

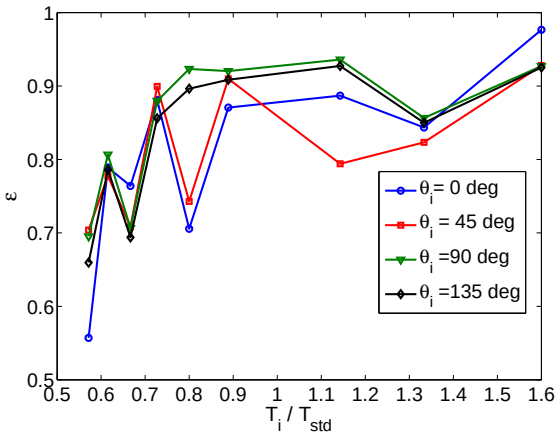

Fig. 10. Hydrodynamic efficiency for each two-component incident wave simulation.

simulation. This highlights the additional complexity associated with effective energy extraction from a realistic irregular incident wave field.

To determine the wave components in the resulting wave field at the up- and down- wave boundary an FFT analysis was performed on both multi-component incident wave simulations. The results for each simulation are shown in Figs.11(c) and 12(c), respectively. The FFT results in Fig. 11(c) indicate that the CycWEC is effectively canceling all 7-components of the incident wave field simultaneously. As such, the hydrodynamic efficiency for this simulation was $\epsilon = 0.85$. The FFT results in Fig. 12(c) indicate that the CycWEC is effectively canceling the first 7-components of the incident wave field (i.e., $W_{I1} - W_{I7}$), while components 8-10 (i.e., $W_{I8} - W_{I10}$)are passing the CycWEC relatively undisturbed. As such, the hydrodynamic efficiency for this simulation was somewhat lower, at $\epsilon = 0.77$, but still very encouraging given the complexity of the incident wave field.

IV. Conclusion

Inviscid numerical simulations were conducted to determine the cycloidal wave energy converter performance in irregular unidirectional deep ocean waves. Initial wave generation simulations demonstrated that a single CycWEC can generate single sided waves with frequencies ranging from 0.4 rad/s to 1.12 rad/s by varying the device rotational period. This frequency range spans the wave frequencies that transport the majority of the wave energy in typical deep ocean wave spectra. The efficient cancellation of irregular deep ocean waves was also demonstrated. This was accomplished by controlling the position of the CycWEC hydrofoils and bound circulation using the feedback flow-control. Initial simulations with an irregular incident wave field consisting of two regular wave components superimposed demonstrated the ability to effectively extract energy from multiple wave components simultaneously. The hydrodynamic efficiency for these simulations ranged from 0.57 to 0.98, but for most simulations was greater than 0.80. To determine the CycWEC performance in more realistic irregular unidirectional deep ocean wave fields, simulations were completed with incident wave fields consisting of 7- and 10-regular wave components. Hydrodynamic efficiencies for these simulations were 0.85 and 0.77, respectively. Thus the CycWEC has the potential to operate effectively in irregular unidirectional deep ocean waves. All of the results presented here will be validated against 1/10 scale experiments that will begin in 2011 at the Texas A&M Offshore Technology Research Center .

Acknowledgment

This material is based upon work supported by the Department of Energy under Award Number DE-EE0003635.

Disclaimer

References

[1] S. G. Siegel, T. L. Jeans, and T. E. McLaughlin, "Deep ocean wave energy conversion using a cycloidal turbine," *Applied Ocean Research*, vol. 33, no. 2, pp. 110–119, 2011.

[2] S. G. Siegel, T. L. Jeans, and T. E. McLaughlin, "Intermediate ocean wave termination using a cycloidal wave energy converter," in *Proceedings of 29th International Conference on Ocean, Offshore and Artic Engineering*, no. OMAE2010-20030, Shanghai, China, 2010.

[3] J. Pinkster and A.J.Hermans, "A rotating wing for the generation of energy from waves," in *22nd IWWWFB Conference, Plitvice, Croatia*, 2007.

[4] C. Marburg, "Investigation on a rotating foil for wave energy conversion," Master's thesis, TU Delft, 1994.

[5] A. J. Hermans, E. van Sabben, and J. Pinkster, "A device to extract energy from water waves," *Applied Ocean Research Computational Mechanics Publications*, vol. Vol. 12, No. 4, p. 5, 1990.

[6] E. van Sabben, "De in het snelheidsveld van lopende golven rond-draaiende plaat; invloed op het vrije vloeistofoppervlak," Master's thesis, TU Delft, 1987.

[7] S. G. Siegel, M. Roemer, J. Imamura, C. Fagley, and T. E. McLaughlin, "Experimental wave generation and cancellation with a cycloidal wave energy converter," in *Proceedings of 30th International Conference on Ocean, Offshore and Artic Engineering*, no. OMAE2011-49212, Rotterdam, The Netherlands, 2011.

[8] J. N. Newman, *Marine Hydrodynamics*. MIT Press, 1977.

[9] J. Wehausen and E. Laitone, *Surface Waves, Handbook of Physics, Vol.9*. Springer-Verlag, 1960.

[10] K. McTaggart, "Modelling and simulation of seaways in deep water for simulation of ship motions," Defence R&D Canada - Atlantic, Tech. Rep. DRDC Atlantic TM 2003-190, September 2003.

[11] "ITTC seakeeping committee report," in *15th International Towing Tank Conference, The Hauge, The Netherlands*, 1978.

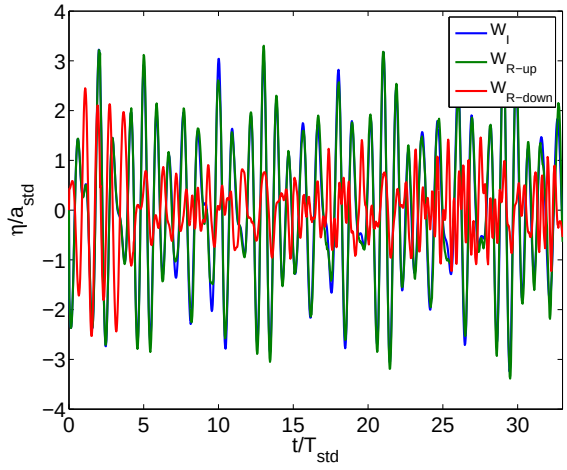

(a) Resulting surface elevation at $x = \pm\lambda_{std}$.

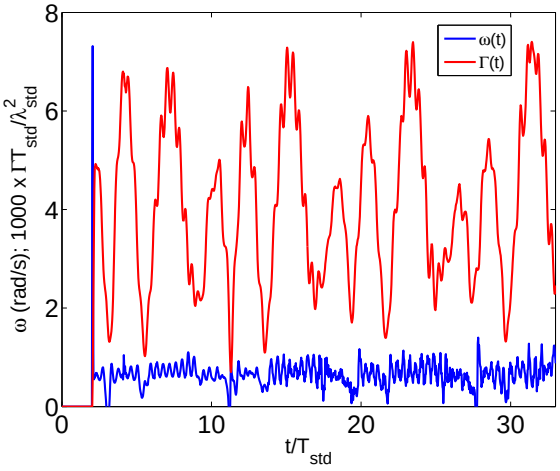

(b) Hydrofoil circulation and angular rotation rate.

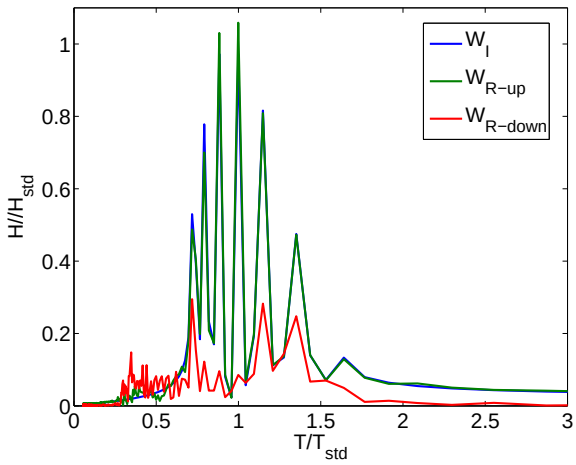

(c) FFT analysis of incident and resulting wave fields at $x = \pm\lambda_{std}$.

Fig. 11. Simulation results for the 7-component incident wave field, $W_I = \sum_{i=1}^{7} W_i$, each with a random phase, θ_i, based on a uniform distribution between 0 and 2π. The calculated hydrodynamic efficiency was $\epsilon = 0.85$.

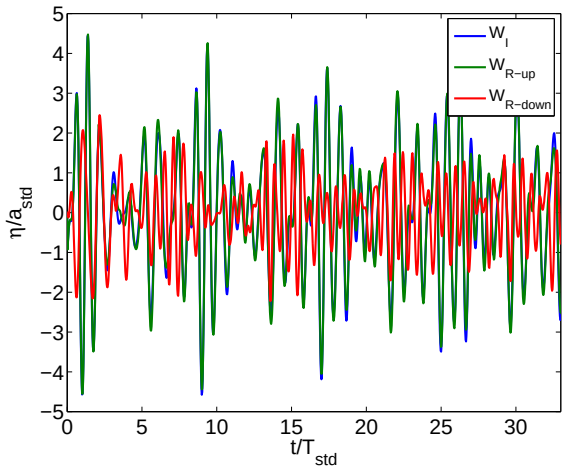

(a) Resulting surface elevation at $x = \pm\lambda_{std}$.

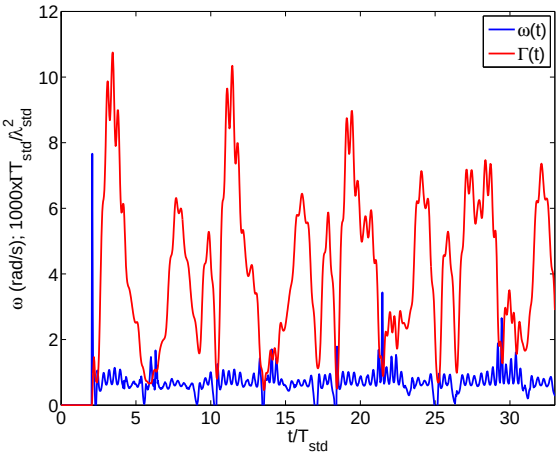

(b) Hydrofoil circulation and angular rotation rate.

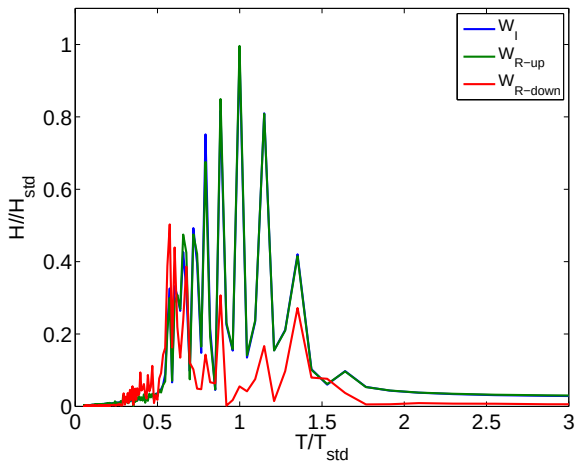

(c) FFT analysis of incident and resulting wave fields at $x = \pm\lambda_{std}$.

Fig. 12. Simulation results for a 10-component incident wave field, $W_I = \sum_{i=1}^{10} W_i$, each with a random phase, θ_i, based on a uniform distribution between 0 and 2π. The calculated hydrodynamic efficiency was $\epsilon = 0.77$.